Interstitial doping effect on ferroelectric rhombohedral HfO_2 from *ab initio* simulations

Chang Hoon Kim,[1] Pawan Kumar,[1] and Jun Hee Lee[1,2,*]

[1] *Department of Energy Engineering, School of Energy and Chemical Engineering, Ulsan National Institute of Science and Technology (UNIST), Ulsan 44919, Republic of Korea*

[2] *Graduate School of Semiconductor Materials and Devices Engineering, Ulsan National Institute of Science and Technology (UNIST), Ulsan 44919, Republic of Korea*

(Received 30 May 2025; revised 23 September 2025; accepted 12 November 2025; published 4 December 2025)

The orthorhombic $Pca2_1$ phase of HfO_2 exhibits exceptional ferroelectric stability at the nanoscale, yet its intrinsically high coercive field E_c remains a significant obstacle to practical applications. The recent discovery of an interstitially doped ferroelectric rhombohedral $R3m$ phase in HfO_2 offers a promising route to reducing E_c. However, the atomic-scale mechanisms driving this behavior remain incompletely understood. Here, using phonon analysis combined with density functional theory simulations, we reveal that interstitial doping and compressive strain strengthen the weak trilinear couplings among the phonon modes that condense in the $R3m$ phase and induced additional modes. These enhanced couplings dramatically increase the polarization, enabling switching at a remarkably low E_c. Our first-principles simulations show that the polarization response strongly depends on the interstitial dopant, as Ti induces large polarization under a slight compressive strain, while Ce, Hf, and Zr require a threshold strain to trigger a polarization jump. Interestingly, we further show that all group-IV interstitial dopants remarkably reduce the E_c under compressive strain. These insights demonstrate that interstitial doping, combined with compressive strain, is a powerful strategy for tuning the ferroelectric properties of HfO_2 and offers a promising pathway to enhanced polarization and reduced switching barriers in next-generation ferroelectric devices.

DOI: 10.1103/xcgt-crgs

I. INTRODUCTION

The discovery of ferroelectricity in the $Pca2_1$ phase of HfO_2 [1] has garnered significant attention from both academia and industry due to its unprecedented switchable polarization in ultrathin films [2–4] and compatibility with complementary metal-oxide semiconductor technology [5,6]. Since then, HfO_2-based ferroelectrics have demonstrated remarkable properties, including scalability down to a few nanometers [2,7] and high endurance [8], positioning them as promising candidates for next-generation nonvolatile memory [9] and low-power logic applications [5]. However, they suffer from a high coercive field, exceeding 1 MV/cm [10] in polycrystalline films and reaching 2–5 MV/cm [11,12] in epitaxial films, which can degrade device reliability and limit endurance. Consequently, strategies to reduce the coercive field without compromising ferroelectric performance are of great interest [13–15]. In recent years, both theoretical and experimental studies have been conducted to lower the coercive field in the ferroelectric $Pca2_1$ phase of HfO_2 through doping [4,16], strain [17], oxygen vacancies [18], and interface engineering [14,19]. However, these efforts have met with only limited success. Other ferroelectric phases, such as orthorhombic $Pmn2_1$ and rhombohedral $R3m$ [11,20], have also been identified in HfO_2, but they remain metastable and are difficult to stabilize under ambient conditions.

A recent experimental study on the $R3m$ phase, which exhibits very poor ferroelectricity in pristine HfO_2, has demonstrated that interstitial doping can induce strong ferroelectricity and drastically reduces the coercive field to as low as approximately 0.65 MV/cm in HfO_2-based ferroelectrics [21]. This ultralow coercive field is attributed to interstitial dopants that stabilize a polar rhombohedral $R3m$ phase of HfO_2 with a much smaller switching barrier. In the $R3m$ structure, the polarization is oriented along the cubic [1 1 1] direction [22]. First-principles calculations suggest that around 8% Hf interstitial doping under approximately 7% compressive strain yields a ferroelectric switching barrier on the order of 7–8 meV/atom [21], significantly lower than the approximately 20-meV/atom barrier in undoped HfO_2. Though the combined effect of interstitial doping and strain leads to impressive ferroelectricity in $R3m$ HfO_2, the atomic-scale mechanism behind this behavior is not yet fully understood, and it is crucial to identify the roles of both interstitial doping and strain.

*Contact author: junhee@unist.ac.kr

In this work, using group theory, phonon analysis, and first-principles simulations, we investigated the interstitial doping effect on the ferroelectric $R3m$ phase of HfO_2. We show that interstitial cations enhance the trilinear couplings among phonon modes that condense in the $R3m$ phase, thereby stabilizing robust ferroelectricity under compressive strain. We not only explain previously reported results of interstitial doping of Hf and Zr in $R3m$ HfO_2, but also successfully apply our analysis to the group-IV element Ti and f-block element Ce, which shares chemical similarities with group-IV elements. Our atomic-scale study is organized as follows: First, we identify the phonon modes involved in the transition from the reference cubic phase to the ferroelectric $R3m$ phase in pristine HfO_2, along with their couplings that drive this phase transition. Next, we examine the impact of interstitial doping and strain on the phonon modes of the parent cubic phase, providing insight into how dopants and strain influence the nonpolar $R\bar{3}m$ phase, which serves as the transition state of the ferroelectric $R3m$ phase. We then investigate changes in polarization and phonon mode amplitudes in the $R3m$ phase as a function of compressive strain for each dopant. Moreover, we evaluate the ferroelectric switching energy barrier for both the doped and undoped $R3m$ phase under varying levels of strain, discussing the implications for coercive field and device performance. Finally, we extend our study to various interstitial dopants across the periodic table, which further validates our analysis. Thus, our study provides valuable guidelines for leveraging interstitial doping and strain engineering to enhance ferroelectric HfO_2, thereby advancing its potential in applications such as nonvolatile ferroelectric memory.

II. COMPUTATIONAL DETAILS

We performed first-principles calculations within the density functional theory based on a plane-wave pseudopotential scheme implemented in the Vienna *ab initio* simulation (VASP) [23–27]. The projector augmented wave [28] pseudopotential with a generalized gradient approximation and the revised Perdew-Burke-Ernzerhof for solid [29] form of exchange-correlation energy functional were used with the $5s^2 5p^6 6s^2 5d^2$ electronic states of Hf and $2s^2 2p^4$ states of O as valence states. The $5s^2 5p^6 4f^1 5d^1 6s^2$ electronic states for dopant Ce, the $4s^2 4p^6 4d^2 5s^2$ electronic states for dopant Zr, and the $3s^2 3p^6 3d^3 4s^1$ electronic states for dopant Ti were used. The energy cutoff to truncate the plane-wave basis sets in representing Kohn-Sham wave functions was set to 500 eV. The k-point meshes were sampled using the Monkhorst-Pack scheme [30] with $8 \times 8 \times 8$ for the cubic cell and $6 \times 6 \times 5$ for the hexagonal lattice. All structural relaxations were performed with a force convergence criterion of 0.01 eV/Å and an energy convergence criterion of 10^{-8} eV. We estimated spontaneous polarization [31,32] of ferroelectric $R3m$ phase by multiplying the Born effective charge Z^* with the atomic displacements d from the centrosymmetric cubic phase as follows:

$$P_s = \frac{e}{V} \sum_i Z_i^* \cdot d_i, \tag{1}$$

where e and V represent the electronic charge and supercell volume, respectively, while i denotes the atomic site in the supercell. To estimate the phonon mode amplitudes condensed in different phases of HfO_2, we used a scheme reported in Ref. [33].

III. RESULTS AND DISCUSSION

The ferroelectric $R3m$ phase emerges as a metastable state when nine distortion modes condense in the reference cubic phase of pristine HfO_2 (Fig. 1). These modes can be categorized into three groups of triply degenerate modes. Among them, the X_2', Y_2', and Z_2' modes are the most unstable in the cubic phase, driving the phase transition to $R3m$ and contributing most significantly. The X_1, Y_1, and Z_1 modes are the highest frequency modes and contribute moderately. In contrast, the polar Γ_{15}^x, Γ_{15}^y, and Γ_{15}^z modes contribute minimally to distortion but induce a net polarization along the [1 1 1] direction, resulting in weak ferroelectricity in the $R3m$ phase of pristine HfO_2. Moreover, six additional symmetrically equivalent nonpolar modes ($X_5^y, X_5^z, Y_5^x, Y_5^z, Z_5^x$, and Z_5^y) (Fig. S1 in the Supplemental Material [34]) also condense with negligibly small amplitudes on the order of 10^{-4} Å (Table S1 in the Supplemental Material [34]) in pristine HfO_2, yet they play an important role by mediating trilinear couplings between polar and unstable modes, which are essential to enhance polarization. Interestingly, similar to the $Pca2_1$ phase, the polar modes in the $R3m$ phase emerge as a secondary order parameter through symmetry-driven trilinear couplings with other nonpolar modes, exhibiting improper ferroelectricity in HfO_2. Symmetrically allowed trilinear phonon-phonon couplings involving unstable modes, along with bilinear and trilinear strain-phonon coupling terms, can be expressed as follows:

$$\begin{aligned} H = {} & a_1(X_2' Y_2' Z_1 + Y'_2 Z_2' X_1 + Z_2' X_2' Y_1) \\ & + a_2(X_2' X_5^y \Gamma_{15}^z + X_2' X_5^z \Gamma_{15}^y + Y_2' Y_5^z \Gamma_{15}^x + Y_2' Y_5^x \Gamma_{15}^z \\ & + Z_2' Z_5^x \Gamma_{15}^y + Z_2' Z_5^y \Gamma_{15}^x) \\ & + g_1(\Gamma_{25}^x \epsilon_{yz} + \Gamma_{25}^y \epsilon_{zx} + \Gamma_{25}^z \epsilon_{xy}) \\ & + g_2(\Gamma_{15}^y \Gamma_{15}^z \epsilon_{yz} + \Gamma_{15}^z \Gamma_{15}^x \epsilon_{zx} + \Gamma_{15}^x \Gamma_{15}^y \epsilon_{xy}), \end{aligned} \tag{2}$$

where a_1 and a_2 are the trilinear phonon-phonon coupling constants, and g_1 and g_2 are bilinear and trilinear strain-phonon coupling constants, respectively. These couplings

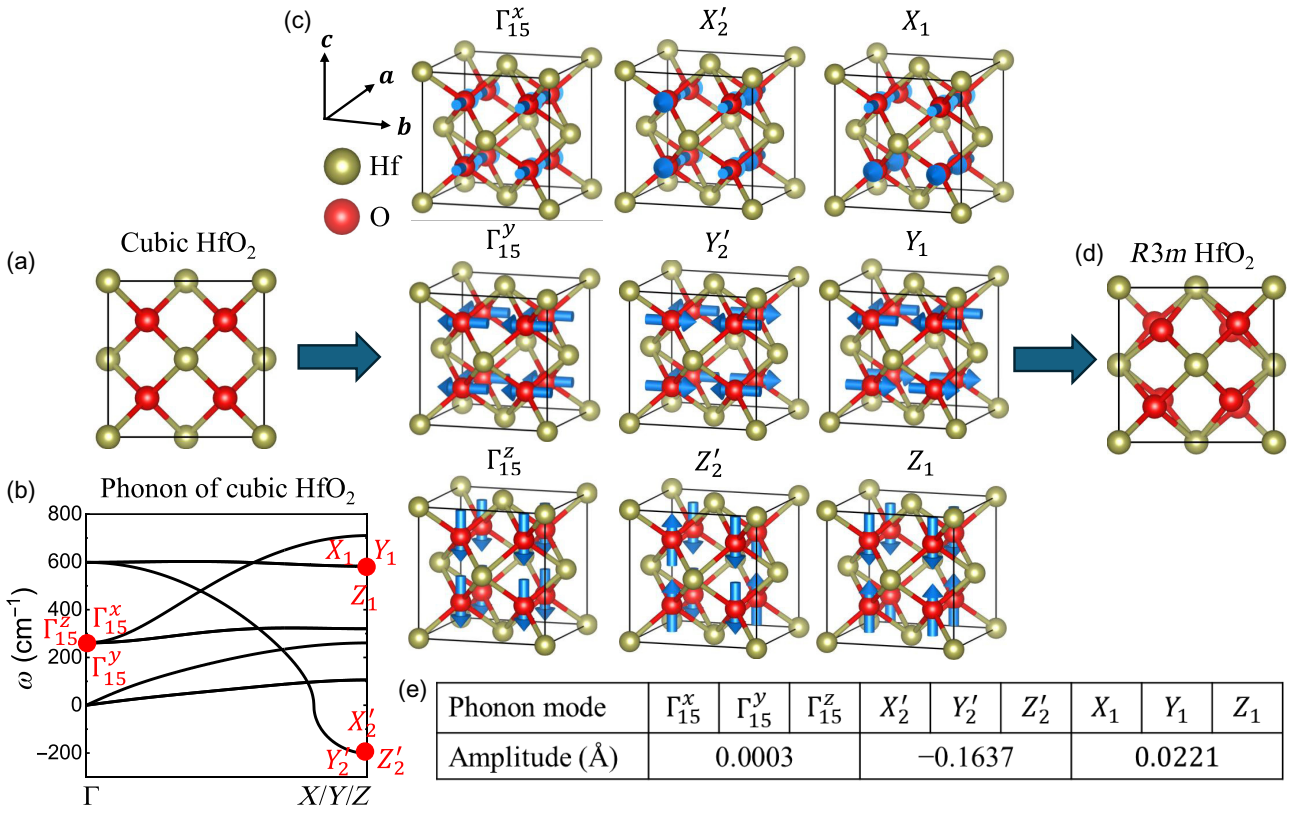

(e)

Phonon mode	Γ^x_{15}	Γ^y_{15}	Γ^z_{15}	X'_2	Y'_2	Z'_2	X_1	Y_1	Z_1
Amplitude (Å)	0.0003			−0.1637			0.0221		

FIG. 1. Atomic structure visualization of 12-atom conventional unit cell of the cubic reference phase of HfO_2 (a). The phonon dispersion of a primitive unit cell of the cubic phase (b). Visualization of atomic displacement of phonon modes (c) that condense in the rhombohedral ($R3m$) phase. The atomic structure visualization of 12-atom unit cell of $R3m$ phase in HfO_2 (d). The amplitude of phonon modes that condense in the $R3m$ phase (e).

play a crucial role in enhancing polarization under compressive strain and interstitial doping (discussed later in the manuscript). The remaining auxiliary trilinear couplings are listed in Eq. (S1) in the Supplemental Material [34].

The rhombohedral $R3m$ phase in pristine HfO_2 stabilizes as a metastable phase [21,22], and its phonon dispersion (Fig. S2 in the Supplemental Material [34]) reveals a phonon instability at the Γ point, which further confirms this and is in very good agreement with earlier theoretical results [22]. We estimated the polarization of $R3m$ HfO_2 to be 0.01 μ C/cm^2 along the [1 1 1] direction. As expected, this value is negligible compared to the typical ferroelectric polarization of 20–30 μC/cm^2 observed in $Pca2_1$ HfO_2-based films. The negligible polarization in the $R3m$ phase is the result of weak trilinear couplings between polar and triple-degenerate unstable modes in pristine HfO_2. However, our analysis suggests that polarization can be enhanced by applying a shear strain, as it directly couples with polar modes [Eq. (2)]. Moreover, if the trilinear couplings between polar and unstable modes become strong, they could potentially lead to enhanced polarization. Therefore, additional perturbations are required to enhance the polar distortion in the $R3m$ phase of HfO_2 to achieve robust ferroelectricity. We thus explore two such perturbations, (a) interstitial doping and (b) compressive shear strain, to stabilize robust ferroelectricity in the $R3m$ phase.

Before directly examining the effects of interstitial doping and strain on the ferroelectric $R3m$ phase, we first investigate their impact on the reference cubic phase of HfO_2 to highlight the important insights regarding the emergence of new phonon modes due to these perturbations in the reference phase itself, which provides insight into whether these perturbations favor its transition to the $R3m$ phase by activating the relevant phonon modes. We show that under the compressive strain applied in the hexagonal a-b plane of the pristine cubic phase [Fig. 2(a)], only the nonpolar Γ^x_{25}, Γ^y_{25}, and Γ^z_{25} modes are induced due to symmetry-allowed bilinear couplings between these modes and the strain [Eq. (2)]. The amplitudes of these modes [Fig. 2(c)] increase with increasing compressive strain, confirming their strong coupling.

We further examine the effect of interstitial doping with the composition $HfM_{0.08}O_2$ (M = Ce, Hf, Zr, and Ti), using the equivalent hexagonal unit cell containing 36 atoms [Fig. 2(b)]. Interstitial doping leads to a different

(a) Cubic HfO_2

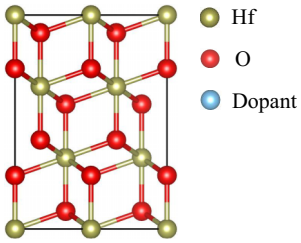

(b) Cubic $HfM_{0.08}O_2$

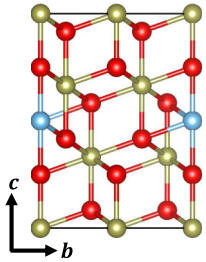

(c)

Strain	d_{111} (Å)	Phonon mode amplitude (Å)	
		X_1, Y_1, Z_1	$\Gamma_{25}^x, \Gamma_{25}^y, \Gamma_{25}^z$
Pristine	2.90	0	0
–2%	2.98	0	−0.0159
–4%	3.06	0	−0.0293
–6%	3.16	0	−0.0387

(d)

Dopant (M)	Phonon mode amplitude (Å)		Material characteristic
	X_1, Y_1, Z_1	$\Gamma_{25}^x, \Gamma_{25}^y, \Gamma_{25}^z$	
Pristine	0	0	Insulator
Ti	0.0041	0.0011	Insulator
Hf	−0.0015	0.0015	Insulator
Zr	−0.0043	0.0013	Insulator
Ce	−0.0144	0.0025	Metal

FIG. 2. Atomic structure visualization of cubic phase of HfO_2 in 36 atoms (12 Hf and 24 O) in the hexagonal lattice (a). Illustration of an interstitially doped cubic HfO_2 phase ($HfM_{0.08}O_2$) in the same hexagonal lattice with the interstitial dopants M at the center of the cell (0, 0, 0.5) (b). Phonon modes activated by compressive strain in the pristine cubic phase of HfO_2 (c), and with different group-IV interstitial dopants at zero strain (d). Cubic phase of HfO_2 remains an insulator with dopants Ti, Hf, and Zr, while it exhibits metallic characteristics with Ce.

set of phonon distortions [Fig. 2(d)]. Interestingly, the interstitial dopant induces six distinct modes in the cubic phase, with X_1, Y_1, and Z_1 also condensed in the $R3m$ phase, while Γ_{25}^x, Γ_{25}^y, and Γ_{25}^z are common under both strain and interstitial doping perturbations. Similar to other phonon modes, the induced nonpolar modes also form trilinear couplings with the polar modes that are already condensed in the $R3m$ phase [Eq. (2)]. This suggests that the combined effect of these perturbations can alter the polar modes, thereby enhancing its ferroelectricity.

After establishing a clear understanding of how strain and interstitial doping affect the reference phase, we now examine their influence on the ferroelectric $R3m$ phase. As expected from the couplings between the polar Γ_{15} modes, strain, and nonpolar Γ_{25} modes, the polarization increases significantly from its pristine value [Fig. 3(a)]. Since shear strain in the cubic lattice directly alters the c lattice parameter of the hexagonal-like unit cell, we evaluate all properties in the $R3m$ phase as a function of d_{111}. We find that in pristine HfO_2, the polarization remains nearly zero between $d_{111} = 3.00$ and 3.06 Å, then increases linearly. For Hf and Zr interstitial doping, the polarization remains negligible up to $d_{111} = 3.00$ Å, after which it exhibits a discontinuous jump and saturates beyond 3.03 Å. This indicates that inducing robust ferroelectricity in Hf- and Zr-interstitially doped $R3m$ phases requires the application of a compressive strain, consistent with previous studies [11,21,35]. Furthermore, according to the previous study of Ref. [36], d_{111} spacing estimation should be considered carefully because even a small mismatch of d_{111} spacing can lead to another phase. Surprisingly, in contrast with other dopants, Ti interstitial doping induces substantial polarization even with lower compressive strain, and this polarization remains sufficiently large across varying strain levels [Fig. 3(a)]. This suggests that Ti is a highly effective interstitial dopant for inducing strong ferroelectricity in the $R3m$ phase without the need for compressive strain.

However, we find that Ce interstitial doping makes the system metallic (Fig. S3 in the Supplemental Material [34]). According to previous reports [37,38], Ce doping results in free electrons, which is the cause of the transition to a metallic state. As a result, polarization is difficult to define, since a metallic material cannot sustain static polarization in the same way as an insulator. Therefore, we exclude the Ce-doped case from the polarization graph. However, we did characterize its structural distortion and found that Ce doping still induces a polar structural distortion under strain [Fig. 3(b)]. Essentially, Ce-doped HfO_2 becomes a polar metallic state, a rare class of materials where a material is metallic yet retains a polar crystal structure. Recent theoretical studies have indeed predicted that HfO_2 can become a polar metal without complete quenching of its polar phonons [39]. Our findings for Ce doping appear consistent with this: free electrons induced by Ce interstitial doping turn HfO_2 into a conductor, but

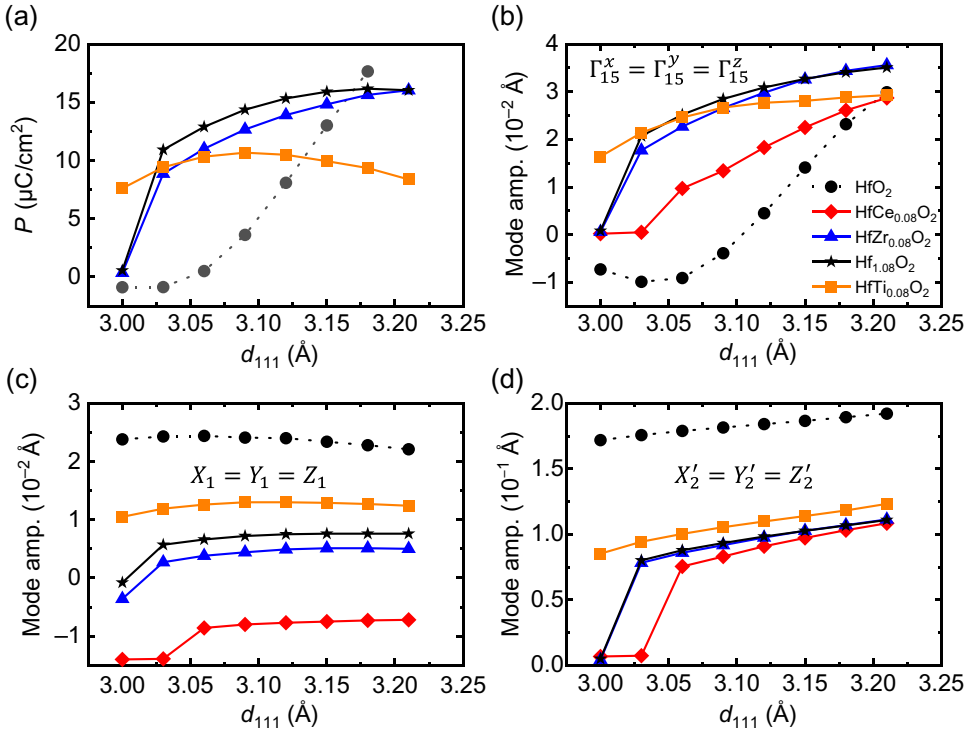

FIG. 3. Estimated polarization (a), triple-degenerate polar modes (b), most stable triple-degenerate nonpolar modes (c), and most unstable triple-degenerate modes (d) versus compressive strain along the [111] direction in the $R3m$ phase of HfO_2 in pristine and different group-IV interstitially doped cases. Ce-doped HfO_2 becomes metallic thus its polarization is omitted; Ti doping yields the highest polarization at low strain; Hf and Zr dopants show negligible polarization at low strain but a sharp increase at the critical strain ($d_{111} = 3.03$ Å); and pristine HfO_2 requires higher strain to polarize strongly, eventually surpassing the doped cases at the largest strain.

the lattice still favors polar distortion. In practice, a polar metal HfO_2 might not be useful for nonvolatile memory (since it would not hold a remanent polarization state), but it could have interesting implications for phenomena like the superconductivity in doped ferroelectrics [39,40].

Further, we examine the effect of compressive strain and interstitial doping on the other modes of the $R3m$ phase. We find that all three degenerate polar modes exhibit the same trend of polarization as a function of compressive strain for both pristine HfO_2 and all interstitial dopants [Fig. 3(b)], emphasizing the linear relationship between the polar modes and the resulting polarization. The Ce-doped case, interestingly, also shows a jump in polar phonon modes at a slightly higher critical strain ($d_{111} = 3.06$ Å); beyond that point, the Ce-doped structure has a polar distortion comparable with the others. This indicates that Ce, Hf, and Zr interstitial dopants require a threshold compressive strain to stabilize polarization in the $R3m$ phase, while, interestingly, Ti exhibits a remarkable polar state at negligible strain.

Figures 3(c) and 3(d) show the behavior of two other phonon mode amplitudes as a function of strain. We observe that for the pristine and Ti-doped cases, the amplitudes of these phonon modes change relatively gradually with strain. In contrast, for the Hf-, Zr-, and Ce-interstitially doped cases, these modes exhibit sudden changes at the same critical strains mentioned above. For instance, at the strain where the Hf and Zr cases underwent the polarization jump, we also see a sharp change in these phonon mode amplitudes. The Ce case similarly shows a distinct change at its critical strain. This suggests that in Hf-, Zr-, and Ce-doped HfO_2, the structural transition at the critical strain involves a concerted change in multiple mode amplitudes, likely a first-order transition where the structure rearranges to a new configuration. On the other hand, the Ti-doped and undoped HfO_2 respond to strain in a more continuous manner, implying a more gradual second-order-like enhancement of the polar distortion without an abrupt phase switching.

Thus, the distortion mode analysis under strain reveals that different interstitial dopants modulate the ferroelectric response of HfO_2 in distinct ways. Ti makes the lattice ready to be polar even with a smaller strain, exhibiting a continuous enhancement of an already-present polar mode as strain increases. Hf and Zr keep the lattice in a metastable polar state, and a critical strain is required to enhance the ferroelectricity in the $R3m$ phase. Ce keeps the system in a nonpolar and metallic state until enough

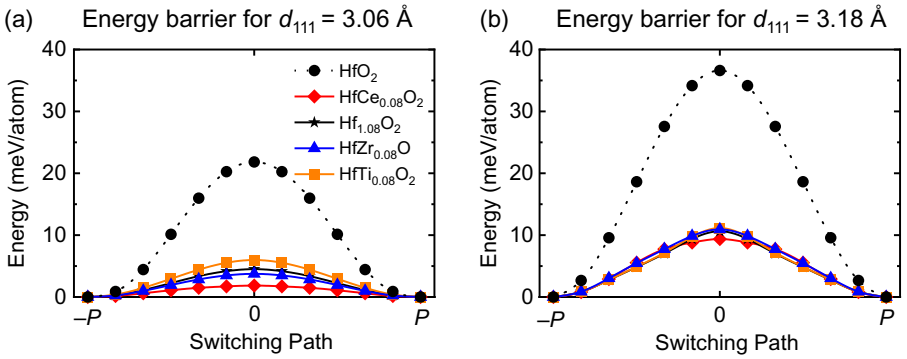

FIG. 4. Ferroelectric switching energy barriers in $R3m$ HfO_2 under compressive strain for different interstitial dopants (a). Energy barrier at a low compressive strain (equivalent to $d_{111} = 3.06$ Å). The barrier is derived from the energy difference between the polar $R3m$ and the nonpolar $R\bar{3}m$ phases along the polarization switching path. The undoped case has the highest barrier, while interstitial dopants drastically reduce the barrier below 10 meV/atom. Energy barrier at a higher compressive strain (equivalent to $d_{111} = 3.18$ Å) (b). At $d_{111} = 3.18$ Å strain, the energy barriers for all dopants slightly increase compared with $d_{111} = 3.06$ Å and almost overlap each other. These comparisons highlight that interstitial doping is most impactful in lowering the switching barrier.

strain is applied, at which point a polar distortion can also emerge. The pristine HfO_2 needs the largest strain to produce significant polarization, but beyond a high strain it can reach a comparable or even higher polarization than doped HfO_2, implying that doping is most useful in the low-to-moderate strain regime to reduce the strain required to stabilize ferroelectricity.

To access the coercive field, which is proportional to the polarization switching energy barrier [33], we calculate the polarization switching barriers for the group-IV interstitially doped $R3m$ phase under different strain conditions [Figs. 4(a) and 4(b)] using the nudged elastic band method implemented in VASP. We find that the polarization switching occurs via the intermediate $R\bar{3}m$ phase (Fig. S4 in the Supplemental Material [34]), which was also found in previous work [22]. In Fig. 4(a), we compare the energy barriers for the undoped and doped systems at a low compressive strain condition. We find that introducing any interstitial dopants remarkably lowers the energy barrier relative to pristine HfO_2. Among the dopants, Ti has a slightly higher barrier than the others, while the Ce interstitial dopant exhibits the smallest energy barrier. While Ti interstitial doping is favorable to stabilize robust ferroelectricity in the$R3m$ phase, the Ce-interstitially doped $R3m$ phase remains in a metallic state. Notably, our first-principles results at low strain corroborate well with the previous report [21], which found that adding interstitial Hf or Zr can reduce E_c to around 0.65 MV/cm in $Hf_{1.08}O_2$, whereas the undoped material typically has an E_c greater than 1 MV/cm. We further show that the energy barriers at a higher compressive strain [Fig. 4(b)] increase compared with those at a lower strain and become almost identical for all four interstitial dopants, while remaining significantly smaller than for pristine HfO_2. Thus, at a large compressive strain, the system's behavior is dominated by the strain, and the specific identity of the interstitial dopant is no longer a major factor for the switching barrier. This also shows that a large external strain not only stabilizes the polar phase but also increases the energy of the nonpolar intermediate phase, which increases the polarization switching energy barriers.

We also perform interstitial doping of Hf, Zr, and Ti at 3.125% and 6.25% interstitial doping concentrations in the $R3m$ phase using a $2 \times 2 \times 2$ supercell [Figs. S5(a) and S5(b) in the Supplemental Material [34]]. Interestingly, we find that at both 3.125% and 6.25% interstitial doping, the polarization remains close to zero, similar to pristine HfO_2, but exhibits a sudden increase at 8.33% (Fig. S5 in the Supplemental Material [34]). Our findings suggest that below 8.33% doping, the trilinear couplings remain weak and thus do not induce sizable polarization. However, 8.33% appears to be a critical doping concentration that induces significant polarization, which can be further enhanced by shear strain.

We further extend our analysis beyond Ce, Hf, Zr, and Ti interstitial dopants and estimate the effects of various dopants on the energy difference between the ferroelectric $R3m$ and centrosymmetric $R\bar{3}m$ phases (Fig. S6 in the Supplemental Materials [34]), which serves as the energy barrier for polarization switching and is directly associated with the coercive field. We find that as the atomic radius increases to around that of a hafnium atom, the $R3m$ phase also stabilizes, since larger atoms induce a greater strain that helps stabilize this phase, further supporting our proposed mechanism. Interestingly, a similar trend was observed for interstitial doping in the ferroelectric $Pca2_1$ phase and its corresponding intermediate nonpolar $P4_2/nmc$ tetragonal phase [36], where dopants with larger atomic radii stabilize the ferroelectric $Pca2_1$ phase over the tetragonal phase.

IV. CONCLUSION

We conducted phonon analysis and first-principles simulations to explain the origin of robust ferroelectricity in the *R*3*m* phase of HfO_2. Our phonon mode analysis reveals the role of each distortion mode condensed in the *R*3*m* phase, and their trilinear couplings with newly emerging modes induced by interstitial doping and compressive strain. These couplings provide insights into the stabilization of polar modes in the *R*3*m* phase. We established that trilinear couplings play a crucial role in enhancing polarization under interstitial doping and compressive strain perturbations. Thus, they can serve as useful descriptors for identifying other interstitial dopants that could further enhance ferroelectricity in the *R*3*m* phase of HfO_2. We found that among all group-IV dopants, Ti induces a large polarization under smaller strain, whereas Hf and Zr require a critical strain to trigger the ferroelectric transition in the *R*3*m* phase, which remarkably reduces the coercive field. Interstitial doping emerges as a powerful tool for engineering ferroelectric properties in HfO_2, complementing traditional approaches such as substitutional doping and epitaxial strain. Our results provide an atomic-scale understanding of the role of interstitial doping, serving as a guide for future experiments aimed at discovering new interstitial dopants to enhance the performance of HfO_2-based memory devices such as ferroelectric random access memory (FeRAM), ferroelectric field effect transistors (FeFETs), and ferroelectric tunnel junctions (FTJs).

ACKNOWLEDGMENTS

This work was supported by Basic Research Laboratory (Grant No. RS-2023-00218799), Nano & Material Technology Development Program (Grants No. RS-2024-00404361), No. RS-2025-24535610, and No. RS-2023-00257666 through the National Research Foundation of Korea (NRF) funded by the Korea government (Ministry of Science and ICT). This work was also supported by Industrial Technology Innovation Program (Grant No. RS-2025-06642983), the Korea Institute for Advancement of Technology (KIAT) grant funded by the Korea Government (MOTIE) (Grant No. P0023703, HRD Program for Industrial Innovation), and the National Supercomputing Center at the Korea Institute of Science and Technology Information (KISTI) with supercomputing resources including technical support (Grants No. KSC-2022-CRE-0075, No. KSC-2022-CRE-0454, No. KSC-2022-CRE-0456, No. KSC-2023-CRE-0547, and No. KSC-2024-CRE-0545).

DATA AVAILABILITY

The data that support the findings of this article are not publicly available. The data are available from the authors upon reasonable request.

[1] T. S. Böscke, J. Müller, D. Bräuhaus, U. Schröder, and U. Böttger, Ferroelectricity in hafnium oxide thin films, Appl. Phys. Lett. **99**, 102903 (2011).

[2] S. S. Cheema, N. Shanker, S.-L. Hsu, Y. Rho, C.-H. Hsu, V. A. Stoica, Z. Zhang, J. W. Freeland, P. Shafer, C. P. Grigoropoulos, *et al.*, Emergent ferroelectricity in subnanometer binary oxide films on silicon, Science **376**, 648 (2022).

[3] S. S. Cheema, D. Kwon, N. Shanker, R. D. Reis, S.-L. Hsu, J. Xiao, H. Zhang, R. Wagner, A. Datar, M. R. McCarter, *et al.*, Enhanced ferroelectricity in ultrathin films grown directly on silicon, Nature **580**, 478 (2020).

[4] Y. Yun, P. Buragohain, M. Li, Z. Ahmadi, Y. Zhang, X. Li, H. Wang, J. Li, P. Lu, L. Tao, *et al.*, Intrinsic ferroelectricity in Y-doped HfO_2 thin films, Nat. Mater. **21**, 903 (2022).

[5] A. I. Khan, K. Chatterjee, B. Wang, S. Drapcho, L. You, C. Serrao, S. R. Bakaul, R. Ramesh, and S. Salahuddin, Negative capacitance in a ferroelectric capacitor, Nat. Mater. **14**, 182 (2015).

[6] Uwe Schroeder, Min Hyuk Park, Thomas Mikolajick, and Cheol Seong Hwang, The fundamentals and applications of ferroelectric HfO_2, Nat. Rev. Mater. **7**, 653 (2022).

[7] M. H. Park, H. J. Kim, Y. J. Kim, Y. H. Lee, T. Moon, K. D. Kim, S. D. Hyun, and C. S. Hwang, Study on the size effect in $Hf_{0.5}Zr_{0.5}O_2$ films thinner than 8 nm before and after wake-up field cycling, Appl. Phys. Lett. **107**, 192907 (2015).

[8] M. H. Park, H. J. Kim, Y. J. Kim, W. Jeon, T. Moon, and C. S. Hwang, Ferroelectric properties and switching endurance of $Hf_{0.5}Zr_{0.5}O_2$ films on TiN bottom and TiN or RuO_2 top electrodes, Phys. Status Solidi RRL **8**, 532 (2014).

[9] D. S. Jeong and C. S. Hwang, Nonvolatile memory materials for neuromorphic intelligent machines, Adv. Mater. **30**, 1704729 (2018).

[10] M. H. Park, Y. H. Lee, H. J. Kim, Y. J. Kim, T. Moon, K. D. Kim, J. Müller, A. Kersch, U. Schroeder, T. Mikolajick, *et al.*, Ferroelectricity and antiferroelectricity of doped thin HfO_2-based films, Adv. Mater. **27**, 11 (2015).

[11] Y. Wei, P. Nukala, M. Salverda, S. Matzen, H. J. Zhao, J. Momand, A. S. Everhardt, G. Agnus, G. R. Blake, P. Lecoeur, *et al.*, A rhombohedral ferroelectric phase in epitaxially strained $Hf_{0.5}Zr_{0.5}O_2$ thin films, Nat. Mater. **17**, 1095 (2018).

[12] J. Guo, L. Tao, X. Xu, L. Hou, C.-W. Nan, S. Du, C. Chen, and J. Ma, Rhombohedral *R*3 phase of Mn-doped $Hf_{0.5}Zr_{0.5}O_2$ epitaxial films with robust ferroelectricity, Adv. Mater. **21**, 2406038 (2024).

[13] M. H. Park, C.-C. Chung, T. Schenk, C. Richter, K. Opsomer, C. Detavernier, C. Adelmann, J. L. Jones, T. Mikolajick, and U. Schroeder, Effect of annealing ferroelectric HfO_2 thin films: *In situ*, high temperature x-ray diffraction, Adv. Electron. Mater. **4**, 7 (2018).

[14] S. S. Cheema, N. Shanker, L.-C. Wang, C.-H. Hsu, S.-L. Hsu, Y.-H. Liao, M. S. Jose, J. Gomez, W. Chakraborty, W. Li, *et al.*, Ultrathin ferroic HfO_2—ZrO_2 superlattice gate stack for advanced transistors, Nature **604**, 65 (2022).

[15] J. S. Kim, N. Strkalj, A. Silva, V. Lenzi, L. Marques, M. O. Hill, Z. Yuan, Y.-X. Liu, M. T. Becker, S. M. Fairclough, *et al.*, Coercive field control in epitaxial ferroelectric $Hf_{0.5}Zr_{0.5}O_2$ thin films by nanostructure engineering, ACS Appl. Mater. Interfaces **17**, 17 (2025).

[16] T. Li, M. Ye, Z. Sun, N. Zhang, W. Zhang, S. Inguva, C. Xie, L. Che, Y. Wang, S. Ke, *et al.*, Origin of ferroelectricity in epitaxial Si-doped HfO_2 films, ACS Appl. Mater. Interfaces **11**, 4 (2019).

[17] S.-T. Fan, Y.-W. Chen, and C. W. Liu, Strain effect on the stability in ferroelectric HfO_2 simulated by first-principles calculations, J. Phys. D: Appl. Phys. **53**, 23 (2020).

[18] K. Z. Rushchanskii, S. Blügel, and M. Ležaić, Ordering of oxygen vacancies and related ferroelectric properties in $HfO_{2-\delta}$, Phys. Rev. Lett. **127**, 087602 (2021).

[19] S. Shi, H. Xi, T. Cao, W. Lin, Z. Liu, J. Niu, D. Lan, C. Zhou, J. Cao, H. Su, *et al.*, Interface-engineered ferroelectricity of epitaxial $Hf_{0.5}Zr_{0.5}O_2$ thin films, Nat. Commun. **14**, 1780 (2023).

[20] J. P. B. Silva, R. F. Negrea, M. C. Istrate, S. Dutta, H. Aramberri, J. Íñiguez, F. G. Figueiras, C. Ghica, K. C. Sekhar, and A. L. Kholkin, Wake-up free ferroelectric rhombohedral phase in epitaxially strained ZrO_2 thin films, ACS Appl. Mater. Interfaces **13**, 51383 (2021).

[21] Y. Wang, L. Tao, R. Guzman, Q. Luo, W. Zhou, Y. Yang, Y. Wei, Y. Liu, P. Jiang, Y. Chen, *et al.*, A stable rhombohedral phase in ferroelectric $Hf(Zr)_{1+x}O_2$ capacitor with ultralow coercive field, Science **381**, 558 (2023).

[22] W. Ouyang, F. Jia, C. Liu, X. Cheng, Y. Meng, R. Gao, S. Picozzi, and W. Ren, Structural stability and polarization analysis of rhombohedral phases of HfO_2, Appl. Phys. Lett. **123**, 212902 (2023).

[23] G. Kresse and J. Hafner, *Ab initio* molecular dynamics for liquid metals, Phys. Rev. B **47**, 558 (1993).

[24] G. Kresse and J. Furthmüller, Efficient iterative schemes for *ab initio* total-energy calculations using a plane-wave basis set, Phys. Rev. B **54**, 11169 (1996).

[25] G. Kresse and J. Furthmüller, Efficiency of ab-initio total energy calculations for metals and semiconductors using a plane-wave basis set, Comput. Mater. Sci. **6**, 15 (1996).

[26] M. C. Payne, M. P. Teter, D. C. Allan, T. A. Arias, and J. D. Joannopoulos, Iterative minimization techniques for *ab initio* total-energy calculations: Molecular dynamics and conjugate gradients, Rev. Mod. Phys. **64**, 1045 (1992).

[27] G. Kresse and D. Joubert, From ultrasoft pseudopotentials to the projector augmented-wave method, Phys. Rev. B **59**, 1758 (1999).

[28] P. E. Blöchl, Projector augmented-wave method, Phys. Rev. B **50**, 17953 (1994).

[29] J. P. Perdew, K. Burke, and M. Ernzerhof, Generalized gradient approximation made simple, Phys. Rev. Lett. **77**, 3865 (1996).

[30] H. J. Monkhorst and J. D. Pack, Special points for Brillouin-zone integrations, Phys. Rev. B **13**, 5188 (1976).

[31] R. D. King-Smith and D. Vanderbilt, Theory of polarization of crystalline solids, Phys. Rev. B **47**, 1651 (1993).

[32] D. Vanderbilt and R. D. King-Smith, Electric polarization as a bulk quantity and its relation to surface charge, Phys. Rev. B **48**, 4442 (1993).

[33] D. Gupta, P. Kumar, and J. H. Lee, Doping engineering to reduce the coercive field of ferroelectric ZrO_2, Phys. Rev. Appl. **22**, 064039 (2024).

[34] See Supplemental Material http://link.aps.org/supplemental/10.1103/xcgt-crgs for detailed explanation of additional trilinear coupling interactions induced by interstitial doping and compressive strain, phonon dispersion of rhombohedral phase, various interstitial dopants, and different doping concentration effects on ferroelectricity in the rhombohedral phase.

[35] Y. Zhang, Q. Yang, L. T. E. Y. Tsymbal, and V. Alexadrov, Effects of strain and film thickness on the stability of the rhombohedral phase of HfO_2, Phys. Rev. Appl. **14**, 014068 (2020).

[36] T. Zhu, L. Ma, X. Duan, S. Deng, and S. Liu, Origin of interstitial doping induced coercive field reduction in ferroelectric hafnia, Phys. Rev. Lett. **134**, 056802 (2025).

[37] H. Ye, G. Zuo, and Y. Cao, DFT computation of rare earth element doped TiO_2 anatase: Tunable absorption spectra for water splitting application, Chem. Phys. Lett. **828**, 140720 (2023).

[38] M. E. Melo Jorge, M. R. Nunes, R. Silva Maria, and D. Sousa, Metal-insulator transition induced by Ce doping in $CaMnO_3$, Chem. Mater. **17**, 2069 (2005).

[39] Xu Duan and Shi Liu, Emergent superconductivity in doped ferroelectric hafnia, Phys. Rev. B **108**, L241114 (2023).

[40] Y. Tomioka, N. Shirakawa, and I. H. Inoue, Superconductivity enhancement in polar metal regions of $Sr_{0.95}Ba_{0.05}TiO_3$ and $Sr_{0.985}Ca_{0.015}TiO_3$ revealed by systematic Nb doping, npj Quantum Mater. **7**, 111 (2022).